2018

Development and Validation of a Mechanistic Vapor-Compression Cycle Model

Ammar M. Bahman
Ray W. Herrick Laboratories, Purdue University, United States of America, abahman@purdue.edu

Davide Ziviani
School of Mechanical Engineering, Ray W. Herrick Laboratories, Purdue University, dziviani@purdue.edu

Eckhard A. Groll
Purdue University - Main Campus, groll@purdue.edu

Development and Validation of a Mechanistic Vapor-Compression Cycle Model

Ammar M. BAHMAN[1,2,*], Davide ZIVIANI[2], Eckhard A. GROLL[2]

[1]Kuwait University, College of Engineering and Petroleum, Mechanical Engineering Department,
Kuwait City, Kuwait
a.bahman@ku.edu.kw

[2]Purdue University, School of Mechanical Engineering, Ray W. Herrick Laboratories,
West Lafayette, Indiana, USA
abahman@purdue.edu, dziviani@purdue.edu, groll@purdue.edu

* Corresponding Author

ABSTRACT

Detailed models are crucial tools for engineers in designing and optimizing systems. In particular, mechanistic modeling of vapor compression systems for accurate performance predictions at both full- and part-load conditions have been improved significantly in the past decades. Yet, fully deterministic models present still challenges in estimating charge inventory in order to optimize the performance. In this work, a generalized framework for simulating vapor compression cycles (VCC) has been developed with emphasis on a charge-sensitive model. In order to illustrate the capabilities of the tool, a direct-expansion (DX) cycle has been considered. In the cycle model, the compressor was mapped by employing dimensionless π groups correlation proposed by Mendoza-Miranda et al. (2016), the evaporator and the condenser were constructed based on the ACHP models (Bell, 2015). Furthermore, a TXV model was implemented based on Li and Braun (2008) formulation. With respect to the charge inventory estimation, the two-point regression model proposed by Shen et al. (2009) was used to account for inaccurate estimation of refrigerant volumes, ambiguous flow patterns for two-phase flow, and amount of refrigerant dissolved in the oil. The solution scheme required manufacturer input data for each component as well as the amount of refrigerant charge. Hence, the degree of superheating at the evaporator outlet, the subcooling at the condenser outlet and the performance parameters of the VCC system can be predicted. The model was validated with available experimental data available in literature. The simulation results demonstrated that the proposed model is more accurate and more generic than other methods presented in the literature.

1. INTRODUCTION

In recent years, researchers developed several numerical models (both steady-state and dynamic) of direct-expansion (DX) systems to evaluate their performance. However, the application of charge-sensitive mechanistic system models is still lacking. The design and optimization of vapor compression systems are based on the knowledge of the charge inventory, since it strongly influences the overall performance. Furthermore, the use of variable speed equipment, advanced cycle configurations, as well as alternative low-GWP and natural refrigerants require system models that incorporate charge inventory calculations.

The purpose of this study is to develop a detailed mechanistic DX cycle model to predict the system performance by imposing the amount of refrigerant charge, boundary conditions, and by estimating both the subcooling and superheating levels. A 5-ton R-410A single-stage heat pump was tested at different compressor speed to validate the model developed herein. The refrigerant charge predictions are estimated with one- and two-point regression model and compared with the experimental data.

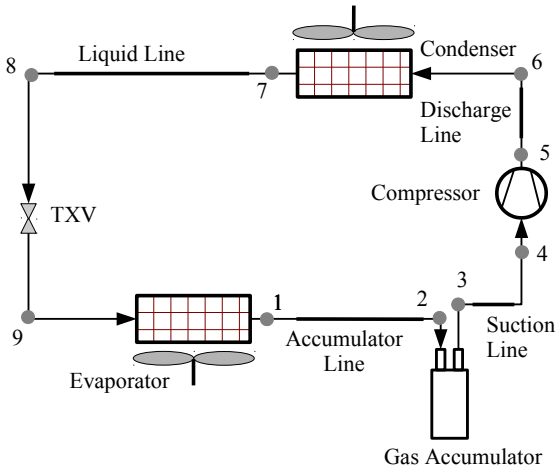

Figure 1: Schematic of mechanistic cycle model that shows the main system components.

2. MODEL DESCRIPTION

Figure 1 shows the schematic of the direct-expansion (DX) heat pump system to be modeled. The cycle components are simulated in an object-oriented fashion by using the programming language Python (2016). The thermo-physical properties of the working fluid (R-410A) were obtained from Bell et al. (2014).

2.1 Compressor Model

A variable speed reciprocating compressors model proposed by Mendoza-Miranda et al. (2016) was used which is based on dimensionless volumetric, isentropic, and overall efficiencies. They have also showed the applicability of the model to scroll and rotary rolling piston compressors. The model characterized the compressor efficiencies in terms of certain groups of dimensionless parameters. Specific experimental data from a 5-ton Hitachi variable speed rotary rolling piston compressor (Figure 2a) were used to determine the values of the dimensionless parameters (*i.e.,* a_i coefficient values, as expressed in Equation 1). Furthermore, the model was capable of accounting for different working fluids. In particular, Mendoza-Miranda et al. (2016) employed the model to analyze the performance of a variable speed reciprocating compressor using R-1234yf, R-1234ze(E), and R-450A as alternatives to R-134a.

$$\pi_1 = a_1 \pi_2^{a_2} \pi_3^{a_3} \pi_4^{a_4} \pi_5^{a_5} \pi_6^{a_6} \pi_7^{a_7} \tag{1}$$

The correlations for the dimensionless efficiencies were expressed as a power law function of the remaining π groups and given in Equations 2 to 4. Table 1 shows the dimensionless groups for volumetric, isentropic, and overall efficiency.

$$\eta_v = \pi_2^{-0.32094} \pi_4^{0.00171} \pi_5^{-0.03695} \tag{2}$$

$$\eta_s = \pi_2^{0.24149} \pi_3^{0.37491} \pi_4^{0.07996} \pi_6^{-0.03367} \tag{3}$$

$$\eta_{oa} = \pi_2^{-0.0136} \pi_3^{-0.07436} \pi_6^{0.18585} \pi_7^{0.6359} \tag{4}$$

The comparisons between measured and predicted values of the compressor mass flow rate, discharge temperature, and electric power input are shown in Figure 3.

2.2 Heat Exchangers Model

The heat exchanger models from Bell (2015) were modified to be used in this work. The condenser model were constructed using a moving boundary method, which divide the heat exchangers according to the phases of refrigerant flow.

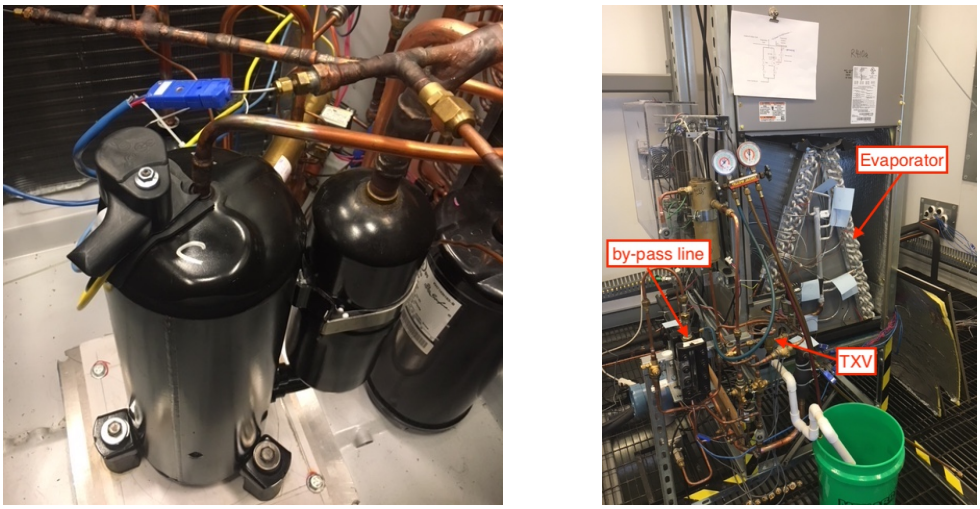

(a) (b)

Figure 2: (a) View of the variable-speed rolling piston compressor; (b) view of the indoor unit.

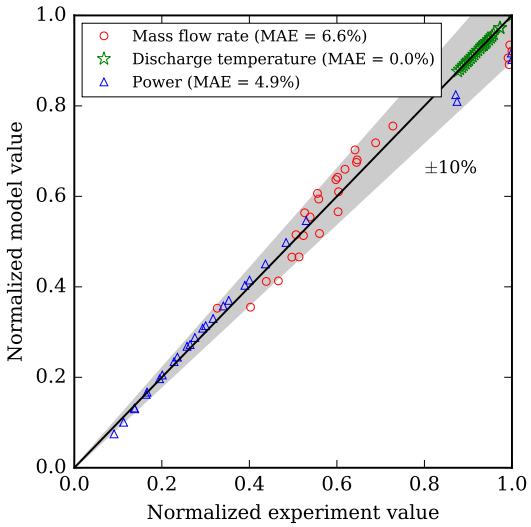

Figure 3: Validation of variable-speed rolling piston compressor.

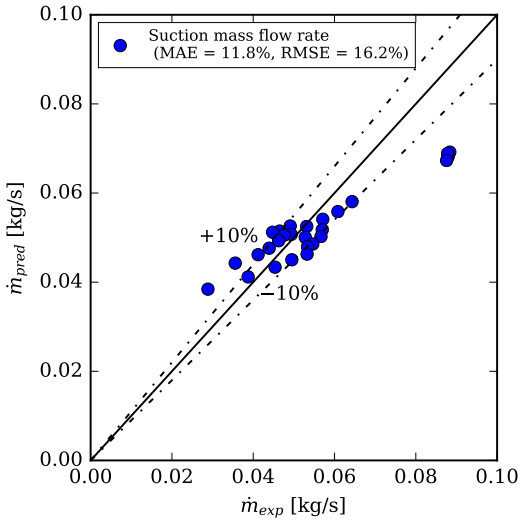

Figure 4: Validation of thermostatic expansion valve (TXV) mass flow model.

Each section of the heat exchanger models were simulated using the ε-NTU method as separate crossflow fin-and-tube heat exchanger (Bergman et al., 2011), assuming constant refrigerant pressure equal to the saturation pressure.

To accurately estimate the behavior of the heat transfer from the air to the refrigerant side of the evaporator, the partially-wet and partially-dry method (Braun, 1988) is utilized in predicting the air side sensible and latent heat transfer when the surface temperature of the coil falls below the dew-point of air at the inlet of the evaporator. The evaporator model was solved by separating the heat exchanger into two sections. The section with surface temperatures higher than the dew-point was solved by a completely dry analysis, while the other section was solved assuming a completely wet analysis.

Both heat exchanger models utilized Zivi (1964) slip flow model to accurately estimate the refrigerant charge in the two-phase region. The correlations used to estimate the heat transfer coefficients and friction factors in the condenser

Table 1: Dimensionless π groups for volumetric, isentropic, and overall efficiencies.

	Volumetric efficiency	Isentropic and overall efficiencies
π_1	η_v	η_s or η_{oa}
π_2	$\frac{P_{dis}}{P_{suc}}$	$\frac{P_{dis}}{P_{suc}}$
π_3	$\left(\frac{\rho_{suc}}{P_{suc}}\right)^{1.5} N_{comp}^3 V_{disp}$	$\frac{N_{ref,comp}}{N_{comp}}$
π_4	$\frac{N_{ref,comp}}{N_{comp}}$	$\frac{N_{comp}^3 V_{disp}}{\Delta h_s^{1.5}}$
π_5	$\frac{M_{\mathrm{R-410A}}}{M_{ref}}$	$\frac{\Delta h_s \rho_{suc}}{P_{suc}}$
π_6	–	$\frac{1}{\frac{(T_{suc}+T_{dis,s})}{2} - T_{amb}}$
π_7	–	$\frac{M_{\mathrm{R-410A}}}{M_{ref}}$

and evaporator models are summarized in Table 2, while the geometrical parameters used are listed in Table 3.

Both evaporator and condenser fans were modeled by using experimental data for steady-state operation conditions. The average airflow rate and power consumption for the evaporator fan were equal to 0.826 m^3/s and 0.4 kW, respectively, while the airflow across the condenser fan was equal to 1.91 m^3/s corresponding to an average measured power consumption of 0.25 kW .

Table 2: Heat transfer and pressure drop correlations in heat exchanger models.

		Single-phase	Two-phase
Refrigerant-side	Heat transfer	Gnielinski (1976)	Condensation: Shah (1979), Evaporation: Shah (1976)
	Pressure drop	Churchill (1977)	Lockhart and Martinelli (1949)
Air-side	Heat transfer	Wang et al. (1998)	
	Fin efficiency	Schmidt (1945) modified by Hong and Webb (1996)	

Table 3: Geometrical parameters in heat exchanger models.

	Condenser	Evaporator
Number of tubes per bank	24	60
Number of banks	2	3
Number of circuits	8	8
Length of tubes [mm]	2252	452
Outer diameter of tubes [mm]	9.13	9.13
Inner diameter of tubes [mm]	8.49	8.49
Longitudinal distance of tubes [mm]	19.1	19.1
Transverse distance of tubes [mm]	25.4	25.4
Fins per inch	20	14.5
Fin waviness [mm]	1.0	1.0
Half-wavelength of fin wave [mm]	1.0	1.0
Fin thickness [mm]	0.11	0.11
Conductivity of fins [W/m-K]	237	117

2.3 Expansions valve Model

An adjustable throat-area device approach was used to model the expansion process for thermostatic expansion valves (TXV). Li and Braun (2008) method was used to model adjustable throat-area expansion valves using experimental rating data. Non-linear model was implemented for the TXV device as expressed in Equations 5. Whereas, the coefficients of the model were tuned using manufacturer's data and summarized in Table 4.

$$\dot{m}_{TXV} = C\left[2\left(\frac{T_{sh}-T_{sh,static}}{T_{sh,max}}\right)-\left(\frac{T_{sh}-T_{sh,static}}{T_{sh,max}}\right)^2\right]\sqrt{\rho_{up}\left(P_{up}-P_{down}\right)} \tag{5}$$

The accuracy of the calibrated mass flow model of the TXV can be seen in Figure 4. The results show a significant under-prediction of the mass flow rate at higher measured values. One of the possible reasons is the absence of pressure data downstream the TXV during the tests. In fact, a by-pass line was installed to test an expander device (see the vertically mounted cylinder in Figure 2b) that introduced significant pressure drops. During the next set of tests, an additional pressure transducer was installed. Nevertheless, it will be shown in Section 3.3 that the overall model was able to predict the mass flow rate reasonably well.

Table 4: Expansion valve model geometrical parameters and mapped coefficients.

D [mm]	9.525
$T_{sh,static}$ [K]	2.626
$T_{sh,max}$ [K]	9.855
C	2.77×10^{-6}

2.4 Linesets Model

The pressure drop of refrigerant flow in the system's pipe linesets were calculated using ACHP model Bell (2015) with the Churchill (1977) correlation to estimate the pressure drop friction factor. The ε-NTU method from Bergman et al. (2011) was used to estimate the amount of heat loss, if any, in all the linesets. Note that the volume of the linesets were considered for the purposed of refrigerant charge calculation. The geometry of the pipelines was measured from the experimental setup and summarized in Table 5.

Table 5: Geometrical parameters of the system linesets.

	Suction line	Discharge line	Liquid line	Accumulator line
Length [mm]	7600	300	7600	571
Outer diameter of tubes [mm]	28.575	28.575	9.525	22.225
Inner diameter of tubes [mm]	26.035	26.035	6.35	19.05
Insulation thickness [mm]	20	–	20	–
Conductivity of tubes [W/m-K]	0.19	0.19	0.19	0.19
Conductivity of insulation [W/m-K]	0.036	–	0.036	–

2.5 Accumulator Model

A suction gas accumulator was modeled as a cylindrical vapor-only container. This implies that natural heat transfer occurred between the surfaces of the accumulator and the surroundings. The natural convection correlations from Bergman et al. (2011) was used to account for the heat transfer across the circumference of the accumulator. Note that the volume of the accumulator was considered for the purposed of refrigerant charge estimation. The accumulator has a height of 274 mm with inner and outer diameters of 115 mm and 123.6 mm, respectively.

2.6 Charge Model

Due to the inaccurate estimation of the system volumes, ambiguous flow patterns under two-phase flow conditions, and amount of refrigerant dissolved in the compressor lubricant, a single-point and a two-point charge tuning procedures

were implemented based on the methodology proposed and validated by Shen et al. (2009). In particular, the total refrigerant charge of the system is given by the sum of the mass calculated by the cycle model and a contribution fitted onto the experimental data which can be expressed as

$$m_{charge} = m_{pred} + \Delta m_{liq} \tag{6}$$

with

$$\Delta m_{liq} = C + K\left(w_{liq,pred} - w_{ref}\right) \tag{7}$$

where C, K, and w_{ref} are the coefficients to be determined through only two experimental data points to calibrate the model. The tunning coefficients are listed in Table 6. Note that for the one-point regression model, Equation (7) results with the coefficient C only.

Table 6: Charge model tunning coefficients.

C [kg]	1.34
K	–2.109
w_{ref}	0.117

2.7 Pre-Conditioner Model

In order to obtain good initial guesses and reduce computational time for the main cycle solver, a pre-conditioner model from Bell (2015) was modified to estimate values for refrigerant evaporation and condensation temperatures. The pre-conditioner model duplicates the main cycle to be solved with simplified models for condenser and evaporator, as shown in Figure 5a. The independent variables (*i.e.,* T_{evap} and T_{cond}) are iterated to minimize the residual vector (Equation 8) by means of *fsolve* function (Moré et al., 1980) until convergence. Note that the superheat degree (*i.e.,* T_{sh}) is deterministically evaluated in the main cycle. However, in the pre-conditioner model a targeted value was used as inputs to ensure continuity.

$$\vec{\Delta} = \begin{bmatrix} \dot{W}_{comp} + \dot{Q}_{evap} - \dot{Q}_{cond} \\ \dot{Q}_{cond,a} - \dot{Q}_{cond,r} \\ \dot{Q}_{evap,a} - \dot{Q}_{evap,r} \end{bmatrix} \tag{8}$$

2.8 System-Level Model

The flow chart in Figure 5b shows the algorithm used in the system-level solver. The components in the system-level model were simulated consecutively as shown in Figure 5b. The independent variables (*i.e.,* T_{evap}, T_{cond}, and T_{sh}) are iterated by means of Broyden (1965) method to drive the residual vector to zero, as expressed in Equation 9.

$$\vec{\Delta} = \begin{bmatrix} m_{charge} - m_{charge,target} \\ h_{evap,out} - h_{accum,in} \\ \dot{m}_{comp} - \dot{m}_{TXV} \end{bmatrix} \tag{9}$$

The model checks for the pressure drop residual after the residual vector converges, as shown in Equation 10. The pressure drops in the high- and low-lineset are considered after the cycle iteration completed to avoid numerical difficulties. Hence, new effective saturation temperatures (*i.e.,* T^*_{cond} and T^*_{evap}) are calculated, and iterated in the cycle model until the updated effective pressure drop (*i.e.,* P^*_{high} and P^*_{low}) are equal to the pressure drop terms calculated from the converged cycle model (*i.e.,* P_{high} and P_{low}).

$$\vec{\Delta P} = \begin{bmatrix} P^*_{high} - P_{high} \\ P^*_{low} - P_{low} \end{bmatrix} \tag{10}$$

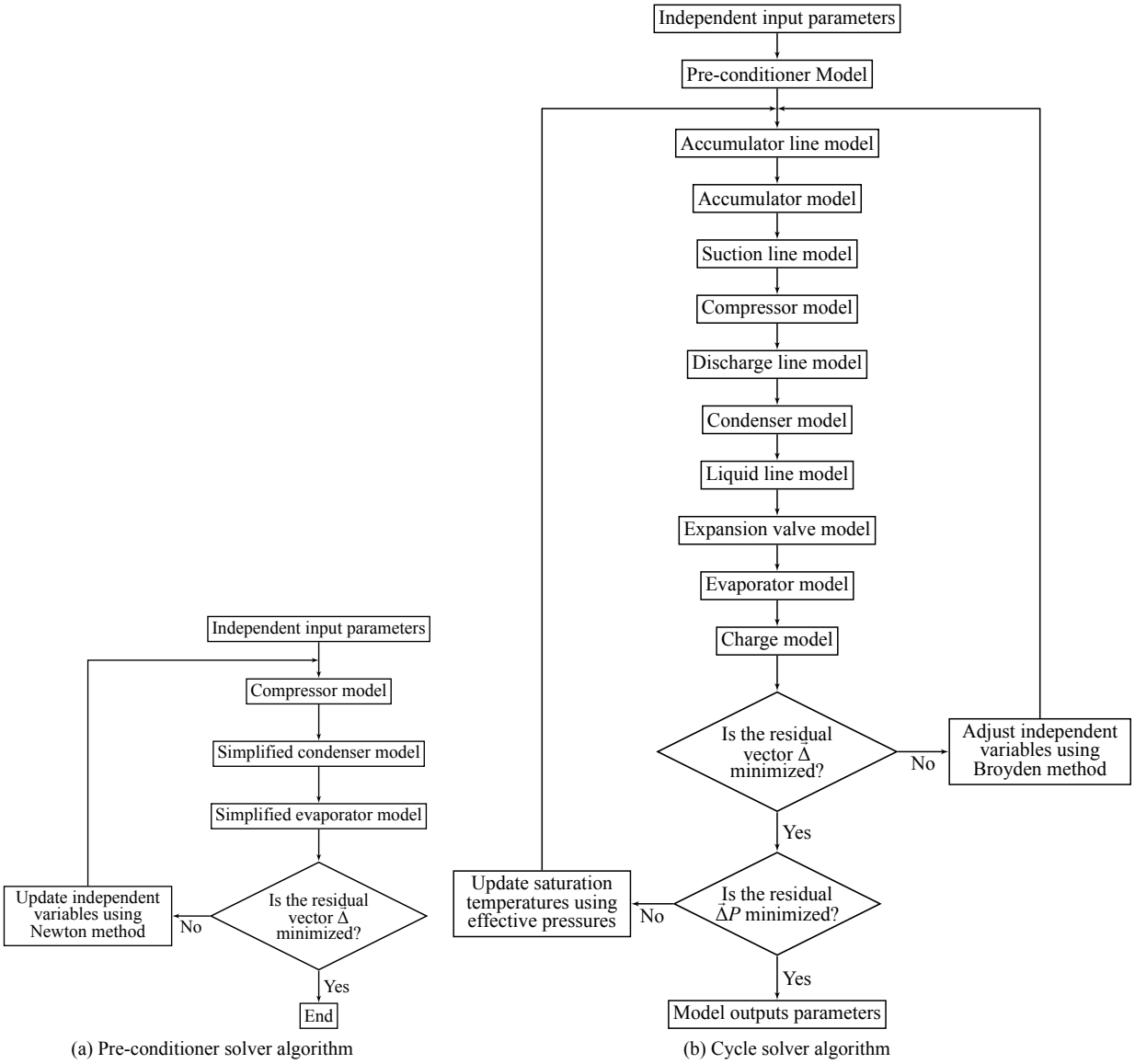

(a) Pre-conditioner solver algorithm (b) Cycle solver algorithm

Figure 5: Flowcharts of pre-conditioner model and mechanistic DX cycle solvers.

3. RESULTS AND DISCUSSION

3.1 Experimental Methodology

A 5-ton single-stage split-type heat pump with R-410A as working fluid was installed inside a pair of psychrometric chambers at the Herrick Laboratories. A variable-speed rolling piston compressor was installed to replace the original scroll compressor. The unit was tested at 26 points according to AHRI Standard 210/240 (Standard, 2008) test conditions in cooling mode for units having variable-speed compressors (*i.e.,* Test Conditions A2, B2, F1, B1, and Ev). The unit was charged with 4.81 kg (10.6 lb) to ensure consistent subcooling in the liquid line.

3.2 Model Tuning

There was a systematic bias between the simulation and experimental results due to simplifications and imperfect information related to the DX system components. To minimize the bias, 7 tuning multipliers were introduced to adjust

mass flow rates, heat transfer coefficients and pressure drop on both air-side and refrigerant-side for the condenser and evaporator model. The estimation of the multipliers was conducted by means of an iterative scheme to eliminate the discrepancy between the experimental results and the estimations of the mass flow rates, the condenser and evaporator heat transfer rates, and the compressor power consumption. The optimization problem was solved with a bounded differential evolutionary (DE) method (Storn and Price, 1997) and the resulted tuning factors are summarized in Table 7.

Table 7: Tuning multipliers for DX system.

Compressor displacement scale factor	0.96
Condenser air-side convection heat transfer coefficient	1.15
Condenser refrigerant-side convection coefficient	1.3
Condenser refrigerant-side pressure drop correlation	0.99
Evaporator air-side convection heat transfer coefficient	1.23
Evaporator refrigerant-side convection coefficient	1.31
Evaporator refrigerant-side pressure drop correlation	0.97

3.3 Model Validation

The validation was carried out with the 26 test conditions which was experimentally conducted on a retrofitted heat pump unit with variable-speed rolling piston compressor. The comparisons of the refrigerant mass flow rate, the condenser and evaporator capacities as well as the compressor and system power consumptions between the model simulations and the experimental results are illustrated in Figure 6. The percentage error between the predicted and experimental values is calculated by the mean absolute error (MAE) and the root mean square deviation (RMSD). Figure 6 shows that the model after tuning captured the system and component performances within a reasonable margin of error. The minimum MAE of 3.0% was corresponded to the total power consumption, while the maximum MAE of 5.7% was associated with the predictions of the cooling capacity.

Using the charge model (Table 6) and the system tuning factors (Table 7), and by imposing the system charge inventory, the cycle was simulated at the same experimental test conditions to assess the charge estimation as shown in Figure 7. Figure 7 compares the charge predictions for the cases without any correction, with one-point regression charge model, and with two-point model. It can be seen that the one-point charge model eliminates all the biases and predicts the charge inventory with MAE and RMSE less than approximately 2.5%, while the two-point charge model (Shen et al., 2009) perfectly estimates the system charge with no errors.

4. CONCLUSIONS

This paper aimed to develop a detailed mechanistic model with a charge-sensitive model for direct-expansion (DX) cycle to accurately estimate the system performance. This way, the system can operate inclusively. The DX system model was tunned and validated with experimental data from a 5-ton single-stage split-type heat pump tested at different compressor speed in the Herrick Laboratories. The results yield the following conclusions:

- The mechanistic DX system model predicted the performance parameters (*i.e.,* mass flow rates, compressor and system powers, and heat exchangers capacities) with a reasonable margin of MAE less than approximately 6%.
- Charge imposed model with one- and two-point correction methods counted for the discrepancy in refrigerant charge estimation with MAE and RMSE less than approximately 2.5%.
- The detailed charge inventory model allows the analyses of drop-in working fluid replacements and their effects on the system sizing. Furthermore, the model also allows to optimize the charge level to take advantage of variable-speed equipment.

ACKNOWLEDGEMENT

The authors would like to acknowledge the support from the Center for High Performance Buildings (CHPB) at the Ray W. Herrick Laboratories.

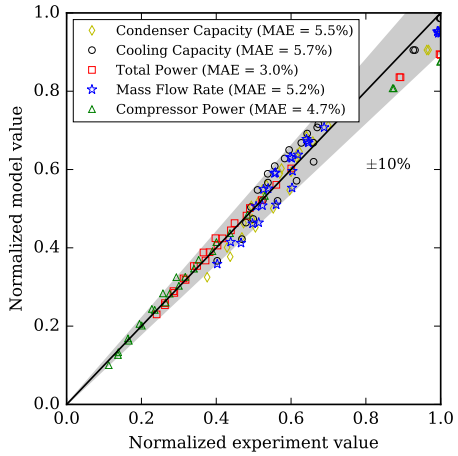

Figure 6: Comparison of estimated model performance parameters with experimental data (normalized with average experimental value).

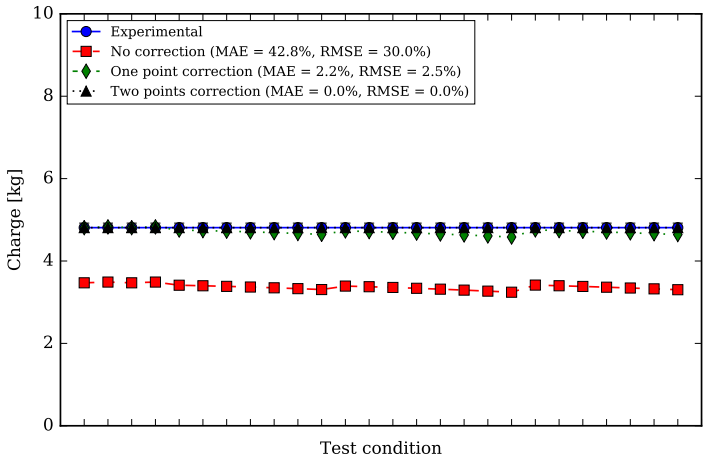

Figure 7: Comparison of charge prediction results with experimental data using one- and two-point regression charge model at different testing conditions.

REFERENCES

Bell, I. H. (2015). Air conditioning and heat pump model (achp) source code version 1.5. [Online; accessed 10-Apr-2018].

Bell, I. H., Wronski, J., Quoilin, S., and Lemort, V. (2014). Pure and pseudo-pure fluid thermophysical property evaluation and the open-source thermophysical property library CoolProp version 6.1.0. *Industrial & Engineering Chemistry Research*, 53(6):2498–2508.

Bergman, T. L., Incropera, F. P., DeWitt, D. P., and Lavine, A. S. (2011). *Fundamentals of heat and mass transfer*. John Wiley & Sons, 7th edition.

Braun, J. E. (1988). *Methodologies for the design and control of central cooling plant*. PhD thesis, University of Wisconsin - Madison.

Broyden, C. G. (1965). A class of methods for solving nonlinear simultaneous equations. *Mathematics of computation*, 19(92):577–593.

Churchill, S. W. (1977). Friction-factor equation spans all fluid-flow regimes. *Chemical engineering*, 84(24):91–92.

Gnielinski, V. (1976). New equations for heat and mass-transfer in turbulent pipe and channel flow. *International chemical engineering*, 16(2):359–368.

Hong, K. T. and Webb, R. L. (1996). Calculation of fin efficiency for wet and dry fins. *HVAC&R Research*, 2(1):27–41.

Li, H. and Braun, J. E. (2008). A method for modeling adjustable Throat-Area expansion valves using manufacturers' rating data. *HVAC and R Research*, 14(4):581–595.

Lockhart, R. and Martinelli, R. (1949). Proposed correlation of data for isothermal two-phase, two-component flow in pipes. *Chemical Engineering Progress*, 45(1):39–48.

Mendoza-Miranda, J. M., Mota-Babiloni, A., Ramírez-Minguela, J. J., Muñoz-Carpio, V. D., Carrera-Rodríguez, M., Navarro-Esbrí, J., and Salazar-Hernández, C. (2016). Comparative evaluation of R1234yf, R1234ze(E) and R450A as alternatives to R134a in a variable speed reciprocating compressor. *Energy*, 114:753–766.

Moré, J., Garbow, B., and Hillstrom, K. (1980). User guide for MINPACK-1.

Python, S. F. (2016). Python language reference, version 2.7.13.

Schmidt, T. (1945). *La production calorifique des surfaces munies d'ailettes*.

Shah, M. M. (1976). A new correlation for heat transfer during boiling flow through pipes. *ASHRAE Transactions*, 82:66–86.

Shah, M. M. (1979). A general correlation for heat transfer during film condensation inside pipes. *International Journal of Heat and Mass Transfer*, 22(4):547–556.

Shen, B., Braun, J. E., and Groll, E. A. (2009). Improved methodologies for simulating unitary air conditioners at

off-design conditions. *International Journal of Refrigeration*, 32(7):1837–1849.
Standard, A. (2008). ANSI/AHRI Standard 210/240. *Performance rating of unitary A/C and air-source heat pump equipment*.
Storn, R. and Price, K. (1997). Differential Evolution - A Simple and Efficient Heuristic for Global Optimization over Continuous Spaces. *Journal of Global Optimization*, 11(4):341–359.
Wang, C.-C., Tsai, Y.-M., and Lu, D.-C. (1998). Comprehensive study of convex-louver and wavy fin-and-tube heat exchangers. *Journal of Thermophysics and Heat Transfer*, 12(3):423–430.
Zivi, S. M. (1964). Estimation of steady-state steam void-fraction by means of the principle of minimum entropy production. *Journal of Heat Transfer*, 86(2):247–251.

NOMENCLATURE

D	Diameter	(m)	**Superscripts**	
h	Enthalpy	(kJ/kg)	*	effective
m	Refrigerant charge	(kg)	**Subscripts**	
$\dot{m}$	Mass flow rate	(kg/s)	*a*	air
M	Molar mass	(kg/mol)	*accum*	accumulator
N	Rotational Speed	(Hz)	*amb*	ambient
P	Pressure	(kPa)	*comp*	compressor
$\dot{Q}$	Heat rate	(kW)	*cond*	condenser
T	Temperature	(°C or K)	*dis*	discharge
V	Volume	(m^3)	*disp*	displacement
w	Area ratio	(–)	*down*	downstream
$\dot{W}$	Power	(kW)	*evap*	evaporator
Acronyms			*exp*	experimental
COP	Coefficient Of Performance	(–)	*in*	inlet
DE	Differential Evolutionary	(–)	*liq*	liquid
DX	Direct Expansion	(–)	*oa*	overall
MAE	Mean Absolute Error	(%)	*out*	outlet
RMSD	Root Mean Square Deviation	(%)	*pred*	predicted
TXV	Thermostatic Expansion Valve	(–)	*r*	refrigerant
Greek symbols			*ref*	reference
Δ	Residual	(units vary)	*s*	isentropic
η	Efficiency	(–)	*sh*	superheated
π	Dimensionless group	(–)	*suc*	suction
ρ	Density	(kg/m^3)	*up*	upstream
ε	Effectiveness	(–)	*v*	volumetric
ζ	Solubility	(–)		